D-band waveguide diplexer fabricated using micro laser sintering

Yang Yu, Yi Wang, Talal Skaik, Thomas Starke, Xiaobang Shang, Michael J. Lancaster, Peter Hunyor, Peter Huggard, Hui Wang, Michael Harris, Mat Beardsley, Qingsha S. Cheng

D-band Waveguide Diplexer Fabricated Using Micro Laser Sintering

Yang Yu, *Member*, *IEEE*, Yi Wang, *Senior Member*, *IEEE*, Talal Skaik, Thomas Starke, Xiaobang Shang, *Senior Member, IEEE*, Michael J. Lancaster, *Senior Member*, *IEEE*, Peter Hunyor, Peter Huggard, Hui Wang, Michael Harris, Mat Beardsley, Qingsha S. Cheng, *Senior Member, IEEE*

Abstract—**We report a D-band waveguide diplexer, with two passbands of 130 - 134 GHz and 151.5 - 155.5 GHz, fabricated using micro laser sintering (MLS) additive manufacturing with stainless-steel. This is the first demonstration of metal 3D printing technology for multi-port filtering device at a sub-THz frequency. For comparison, the same diplexer design has also been implemented using computer numerical controlled (CNC) milling. The diplexer, designed using coupling matrix theory, employs an all-resonator and E-plane split-block structure. The two channels are folded for compactness. A staircase coupled structure is used in one channel to increase the isolation performance. The printed waveguide flanges are modified to adapt to the limited printing volume from the MLS. Effects of fabrication tolerance on the diplexer are investigated. An effective and unconventional electroless plating process is developed. The measured average insertion losses of the gold coated diplexer are 1.31 dB and 1.37 dB respectively. Respective frequency shifts from design values are 0.92% and 1.1%, and bandwidth variations are 4% and 15%. From a comprehensive treatment of the end-to-end manufacture process, the work demonstrates MLS to be a promising fabrication technique for complex waveguide devices at sub-THz frequency range.**

Index Terms—**Additive manufacturing, all-resonator structure, CNC machining, micro laser sintering, surface treatment, waveguide diplexer.**

I. INTRODUCTION

DUE to the generously available bandwidth (up to several tens of GHz) and relatively low atmospheric attenuation, the 110 to 170 GHz D-band has been proposed for applications in high-capacity backhaul links for 5G and beyond [1]-[3]. The

Y. Yu is with the Key Laboratory of Microwave Remote Sensing, National Space Science Center, Chinese Academy of Sciences, Beijing, 100190, China. (email: issacyu@live.cn).

Y. Yu, Y. Wang, Talal Skaik and M. J. Lancaster are with the School of Electrical, Electronic and Systems Engineering, University of Birmingham, Birmingham B15 2TT, U.K. (e-mail: y.wang.1@bham.ac.uk, t.f.skaik@bham.ac.uk, m.j.lancaster@bham.ac.uk).

T. Starke is with the 3D MicroPrint GmbH Technologie, Chemnitz, 09126, DE.

X. Shang is with National Physical Laboratory, Teddington, TW11 0LW, UK.

P. Hunyor, P. G. Huggard, H. Wang, M. Harris and M. Beardsley are with the STFC Rutherford Appleton Laboratory, OX11 0QX, UK.

Q. S. Cheng is with the Department of Electrical and Electronic Engineering, Southern University of Science and Technology, Shenzhen, 518055, P.R. China. (email: chengqs@sustech.edu.cn)
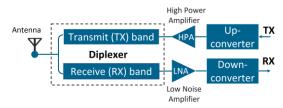

Fig. 1. A block diagram of the diplexer in a communication system.

D-band is also used to remote sensing, for example in space-based radiometers for earth observation [3]. According to European Telecommunications Standards Institute (ETSI) [4], the D-band has a flat and 2 dB lower rain attenuation than the W-band (75-110 GHz). A link distance of several hundred meters is practical at D-Band frequencies with antenna sizes comparable to those at E-Band (60-90 GHz).

One of the essential and most complex passive components in communications system is the antenna diplexer [5]: Fig. 1. The diplexer is a three-port, low loss, filtering component that permits transmit and receive channels, operating at different center frequencies, to share a common antenna. Waveguide technology, with its low loss and a more compact footprint than quasi-optics, is recognized as an excellent choice for sub-THz systems [6]. However, the fabrication of diplexers operating over 100 GHz remains a significant challenge due the performance sensitivity to manufacturing tolerances [6].

Computer numerical controlled (CNC) milling is the most used manufacturing technique for waveguide components [7]-[8]. High precision CNC, with a dimensional tolerance at the level of $\pm 5\,\mu\text{m}$, is required for D-band devices. Components are necessarily fabricated from two or more parts, to allow definition of the waveguide cavities by milling. As well as accurate cavity definition, good surface flatness is needed to ensure contact between the split blocks, and precision alignment features are also required. CNC machining becomes expensive and time consuming when tight tolerances are required [9], and cutter diameters impose minimum limitations on feature radii. Although good performance of waveguide filters has been demonstrated at spot frequencies from 100 GHz to 750 GHz [10]-[16], CNC machining of diplexers is not easy for such high-frequency applications. A CNC-milled G-band, 170-260 GHz, diplexer was realized with an insertion loss of 1.5 dB but a center frequency shift of 3 GHz and bandwidth increase of 30% [7]. A CNC machined hybrid-coupled wideband triplexer at 400 GHz was reported with an insertion loss of 1.75 – 2.63 dB [16].

Other micro-fabrication technologies have emerged for

diplexers operating over 100 GHz, such as silicon deep reactive ion etching (DRIE) [17]-[20], LIGA-based thick-resist electroplating [21]-[22], and multi-layer SU8 process [9], [23]-[25]. These techniques build waveguide components from multiple layers. A WR-3 (220-325 GHz) waveguide diplexer fabricated using SU-8 technology, exhibited significant deviation of insertion loss and bandwidth from predictions [9]. A 300 GHz band diplexer fabricated using a photonic crystal structure achieved an insertion loss of 3 dB [26]. A DRIE D-band diplexer was shown to have very good performance with an insertion loss of 0.8 - 1.2 dB, under 1.4 GHz frequency shift, and around 8% bandwidth deviation from the design [6]. One common challenge of these micro-fabrication techniques is that the multiple layers must be post-process metallized and then assembled with very high alignment accuracy. This increases the complexity and cost. There are also stringent limitations in the design (e.g., limited layer thickness and restrictive choice of usable structures) owing to the materials and processes.

In recent years, additive manufacturing (AM) technology, also known as 3D printing, has emerged as another promising fabrication method for microwave components [28]-[31]. Complex geometries can be relatively easily fabricated. Compared with the above microfabrication techniques, there appear several benefits. 1) The design can be more flexible, and waveguide components can be fabricated in one piece in some cases; 2) For those formed from multiple pieces, the assembly can be simplified and with more flexibility; 3) A single device with different scales of dimensions can be more flexibly produced. Some electrically large sub-THz components (with an overall size of several centimeters) with fine features of several tens of μm can be monolithically fabricated [28]-[30]; 4) Compared with CNC machining, the tooling cost for AM is lower and material wastage is significantly reduced. Horn antennas operating from 60 – 325 GHz were fabricated using binder jetting/sintering of 316L stainless steel and selective laser melting (SLM) on Cu-15Sn bronze [29]. Bandpass filters operating at 90 GHz and 180 GHz were made using a micro laser sintering (MLS) process [30]-[31]. A bent waveguide operating at 140 – 220 GHz made using MLS and a horn antenna at 220 – 320 GHz fabricated using SLM, micro laser sintering (MLS), and metal-coated stereolithography apparatus (SLA) have also been reported [32].

This paper reports a D-band diplexer fabricated using a high-resolution micro laser sintering (MLS) technique on stainless steel [33]. This is the highest frequency diplexer fabricated to date by additive manufacturing technology. Compared with the polymer-based 3D printing technique, metal AM techniques are more suitable for devices requiring higher mechanical and thermal stability. Coupling matrix (CM) theory is applied to design the all-resonator structure [34]-[36]. We chose the conventional rectangular waveguide cavity design in a split-block configuration for several reasons: (1) The split-block configuration is one of the easiest structures in terms of surface treatment (e.g. cleaning, polishing and gold-plating). (2) The open structure allows us to characterizee the print accuracy and surface quality. (3) As part of the
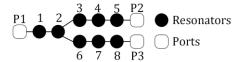

Fig. 2. The coupling topology of the diplexer. Each black node denotes a resonator. The white squares, P1, P2, and P3, represent the ports of the diplexer. The lines between them represent the inter-cavity couplings. Channels A and B correspond to the signal paths P1 to P2 and P1 to P3 respectively.
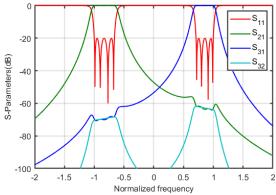

Fig. 3. The calculated S-parameter response from the coupling matrix.

investigation, we also compared the 3D printed diplexer with a conventionally CNC machined diplexer of the same specification and manufactured in the same split-block fashion. This allows us to put the current capability of 3D printing technology into perspective. Comprehensive dimensional, electromagnetic performance and surface quality measurements are performed. The influence of the fabrication tolerance of the micro-printed diplexer is analyzed. Our motivation is to push the boundary of AM to complex waveguide circuits beyond 100 GHz and demonstrate the current capability and limitation through a holistic approach – from design to manufacture, surface treatment and assembly.

The rest of this paper is organized as follows. Section II introduces the diplexer design, including the synthesis and 3D design. Fabrication and assembly are detailed in Section III. Measurements and analyses are presented in Section IV. Section V concludes the work.

II. DIPLEXER DESIGN

A. Filtering topology and coupling matrix synthesis

The diplexer is designed with the following specifications which meet the scope for future communication links reported by ETSI [4] and the frequency bands allocated to fixed service by ITU Radio Regulation 2020 [37].

- *Channel A passband* ($f_{A.1}$ - $f_{A.2}$): 130 - 134 GHz. Return loss $\geq$ 20 dB.
- *Channel B passband* ($f_{B.1}$ - $f_{B.2}$): 151.5 - 155.5 GHz. Return loss $\geq$ 20 dB.
- *Isolation within the passband* $\geq$ 60 dB.

To minimize transmitter power loss and maintain receiver sensitivity, minimum loss in the passbands is required. Different filter orders and topologies have been evaluated. An 8th order all-resonator structure illustrated in Fig. 2 is adopted.

TABLE I
THE OPTIMAL COUPLING COEFFICIENTS FOR THE DIPLEXER

Mutual Couplings		Self-couplings	
$m(1, 2)$	0.8677	$m(1, 1)$	−0.0537
$m(2, 3)$	0.2203	$m(2, 2)$	0.0635
$m(3, 4)$	0.1200	$m(3, 3)$	−0.8021
$m(4, 5)$	0.1548	$m(4, 4)$	−0.8279
$m(2, 6)$	0.1767	$m(5, 5)$	−0.8290
$m(6, 7)$	0.1026	$m(6, 6)$	0.8368
$m(7, 8)$	0.1330	$m(7, 7)$	0.8524
		$m(8, 8)$	0.8537
Input/output Couplings			
$m(1, P1)$	0.5817	$m(5, P2)$	0.4265
$m(8, P3)$	0.3956		

The isolation requirement is met with minimum number of resonators and without complex coupling structures [34]. Without a need of a junction-based frequency distribution network, the diplexer occupies a more compact footprint. All the resonators contribute transmission poles and therefore the selectivity in the passbands. The common resonator-2 also plays a role in frequency distribution.

The coupling matrix synthesis is performed with an optimization-based approach [36]. The optimal coupling values and corresponding normalized scattering parameter responses are given in Table 1 and Fig. 3, respectively. It can be seen that both transmission and rejection requirements are theoretically satisfied.

For the physical realization, the coupling matrix is first transformed into the real-frequency domain. The mutual coupling $m(i, j)$ ($i \neq j$, $i, j =$1, 2, …, 8) and input/output couplings $m(i, Pk)$ ($k =$ 1, 2, and 3) are respectively denormalized by [34]

$$M(i, j) = m(i, j) \cdot FBW \qquad (1)$$

$$M(i, Pk) = m(i, Pk) \cdot \sqrt{FBW} \qquad (2)$$

where $M(i, j)$ and $M(i, Pk)$ are the denormalized mutual couplings and input/output couplings, respectively. The fractional bandwidth of the diplexer FBW is defined as BW/f_0, where BW is the bandwidth and f_0 is the center frequency of the diplexer. For the diplexer in this paper,

$$BW = f_{B.2} - f_{A.1}, \; f_0 = \sqrt{f_{A.1} \cdot f_{B.2}} \qquad (3)$$

where $f_{A.1}$ and $f_{B.2}$ are passband edges, namely $f_{A.1} =$ 130 GHz, $f_{A.2} =$ 134 GHz, $f_{B.1} =$ 151.5 GHz and $f_{B.2} =$ 155.5 GHz. The resonant frequency f_i of the ith asynchronously tuned resonator, related to self-coupling $m(i, i)$, is calculated by [38]

$$f_i = f_0 \left[\left(\frac{m(i,i) \cdot FBW}{2} \right) - \sqrt{1 + \left(\frac{m(i,i) \cdot FBW}{2} \right)^2} \right] \qquad (4)$$

With all the coupling coefficients expressed in the real frequency domain, the physical dimensioning can be executed based on the classical extraction procedure [39]-[40].

B. Structural design and simulation

The air model of the diplexer is illustrated in Fig. 4(a). The diplexer is formed of WR-6 waveguide cavities. Two channels are folded for a compact configuration. An important design feature is that the resonators of Channel A are arranged in a staircase configuration. This makes the overall diplexer more
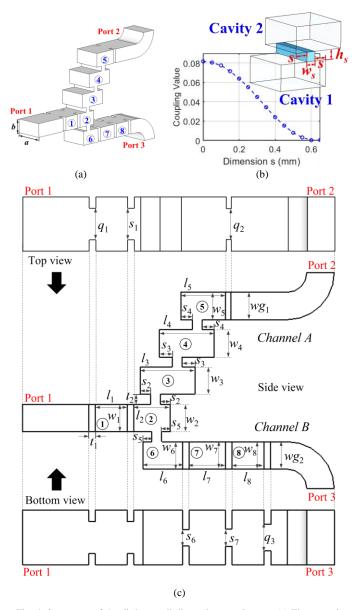

(a)　　　　　　　　　　(b)

(c)

Fig. 4. Structures of the diplexer, all dimensions are in mm. (a) The core air cavity model of the diplexer, $a =$ 1.651 and $b =$ 0.826. (b) Coupling coefficients of two waveguide cavities coupled in a staircase configuration, as a function of s. $w_s =$ 0.300 and $h_s =$ 0.300. (c) Schematic diagram of the diplexer with top view, side view and bottom view. The resonator length: $l_1 =$ 0.958, $l_2 =$1.107, $l_3 =$ 1.654, $l_4 =$ 1.646, $l_5 =$ 1.355, $l_6 =$ 1.184, $l_7 =$ 1.096, $l_8 =$ 0.969. The dimensions related to couplings: $s_1 =$ 0.958, $s_2 =$ 0.304, $s_3 =$ 0.390, $s_4 =$ 0.350, $s_5 =$ 0.261, $s_6 =$ 0.487, $s_7 =$ 0.522. Input/output couplings: $q_1 =$0.959, $q_2 =$0.926, $q_3 =$ 0.795. The thickness for all the irises $t_1 =$ 0.200.

compact and, more importantly, increases the Channel B rejection performance for the P1-P3 path. Fig. 5 shows the performance comparison between a staircase and a linear, inductive iris coupled resonator configuration. Using the staircase configuration, the Channel B isolation is greatly improved to over 60 dB. This is due to the capacitive inter-resonator apertures being positioned so that the coupling between the higher order modes is strongly suppressed [41]. The staircase configuration was not used for the upper channel, as it would slightly worsen the attenuation at the lower stopband.

As shown in Fig. 4(b), to find the coupling coefficient, two

This article has been accepted for publication in IEEE Transactions on Components, Packaging and Manufacturing Technology. This is the author's version which has not been fully edited content may change prior to final publication. Citation information: DOI 10.1109/TCPMT.2022.3204887
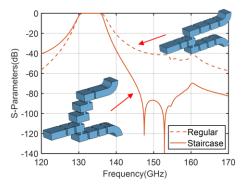
4

Fig. 5. Predicted S-parameter comparison between two diplexers with different configurations in Channel A - a regular inductive iris structure versus a staircase coupled structure.
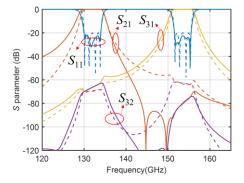

Fig. 6. S-parameter response of the 8th order diplexer shown in Fig. 4 obtained from simulation (solid lines), compared with the theoretical performance calculated using the coupling matrix approach (dashed lines).

TE101 mode cavities are coupled with a slot in the staircase configuration. Their coupling coefficients vary with the offset distance, s, in Fig. 4(b). Considering the fabrication resolution of the additive manufacturing, the height and width of the slot are kept sufficient large and constant at 0.3 mm. The coupling level provided by the slot can fulfil the requirement of the diplexer, since all the couplings in the diplexer are less than 0.08. The physical dimensions are illustrated in Fig. 4(c). Fig. 6 shows the simulated S-parameter responses, obtained from simulation by CST Studio Suite, and compared with the responses calculated from the coupling matrix. The significant improvement in the isolation from the staircase resonators is clearly shown.

As shown in Fig. 7(a), to facilitate the layout of the flanges and accommodate the additive manufacturing using the MLS technique, the three-waveguide ports are extended and bent first along the E-plane and then along the H-plane to permit interfacing with external devices. The diplexer model shown in Fig 7(a) is divided into two halves to be printed. The curved H-plane bends are formed as an integral part of the build, which is not possible with conventional machining techniques. Due to the limitations of the printing volume, parts of the UG387/m flange are removed. The profile of the diplexer model is shown in Fig. 7(b).

As for the CNC machined diplexer, the three ports are extended (without the H-plane bends at the ports) to allow for connection with UG387 flanges as shown in Fig. 7(c). Meanwhile, the corners of the cavities are rounded with a radius
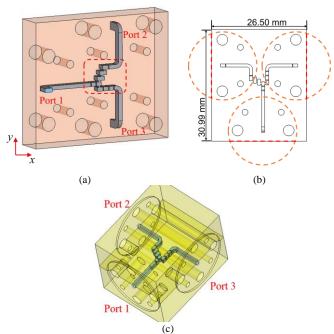

Fig. 7. The diplexer EM design models. (a) The diplexer model for MLS for MLS fabrication with H-plane bends and UG-387 flanges. (b) The top-view profile of the diplexer model for MLS. (c) The diplexer model for CNC milling. The modified dimensions are: the resonator length $l_1 = 0.9238$, $l_2 = 1.1303$, $l_3 = 1.6719$, $l_4 = 1.6650$, $l_5 = 1.3781$, $l_6 = 1.2010$, $l_7 = 1.1002$, $l_8 = 0.9598$. The dimensions related to couplings, $s_1 = 0.9747$, $s_2 = 0.3030$, $s_3 = 0.3918$, $s_4 = 0.3537$, $s_5 = 0.2571$, $s_6 = 0.5156$, $s_7 = 0.5559$. Input/output couplings, $q_1 = 0.9908$, $q_2 = 0.9172$, $q_3 = 0.8369$. Unit: mm.

Fig. 8. The fabrication process of the MLS.

of 0.15 mm to be convenient for milling. The other dimensions are also adjusted as given in the caption of Fig. 7.

III. FABRICATION AND SURFACE TREATMENT

A. Diplexer fabricated by MLS

The diplexer was printed using stainless steel in an inert argon atmosphere on a DMP63 micro printer by 3D MicroPrint GmbH [33]. The fabrication process is illustrated in Fig. 8. Firstly, the CAD model is numerically sliced into layers. During the fabrication, the platform is coated by a thin layer of metal powder, and this is selectively sintered by a focused laser beam. An infrared fiber laser provides a 50 W continuous wave power, with an average power focus diameter of 30 μm. After fusing of one layer, the platform is lowered. Powder covering and selective sintering are repeated until the component is finished. The stainless steel used was 1.4404 (316L), which is chromium-nickel alloyed, containing 17% chromium, 12%

Fig. 9. (a) Photegraphs of the MLS fabricated diplexer components, (b) Photograph of the notch lines on the lower surface of the MLS printed diplexer. (c) The MLS printed diplexer with gold plating. and (d) Photograph of the assembled MLS printed diplexer in the measurment. (e) Photograph of CNC milled diplexer.

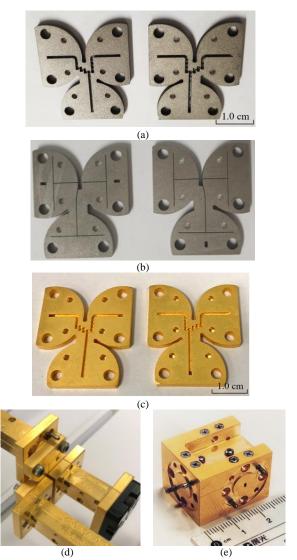nickel, 2% molybdenum, the rest being iron. The thickness of each layer is around 7 µm. The powder particle size, d90, is smaller than 5 µm. The nominal DC electrical conductivity of stainless steel is 1.35×10^6 S/m. It should be noted that the actual electrical conductivity of printed metal after sintering will be different from this. The print took about 30 hours. This could be considerably reduced by further optimizing the build process. The fabricated diplexer parts are shown in Fig. 9(a). The weight of the MLS diplexer is 18.2 g (excluding the screws).

The print of the flat split-block structure is not challenge free. This structure has a very large area-to-thickness ratio, which is prone to thermal stress because of the rapid heating and cooling from the laser-based process (and therefore causing warping if not dealt with). This had to be taken into account in the mechanical design. Notch lines as shown in Fig. 9(b) are added to the lower surface of the structure that is attached to the
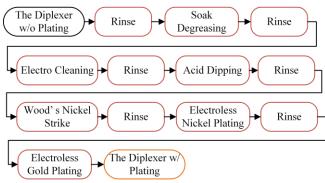

Fig. 10. The workflow of the gold plating process on the MLS diplexer.

printing platform. This helps release the accumulated thermal stress.

As for the CNC machined diplexer (Fig. 7(c)), the manufacture precision is about 10 µm. This was machined on a KERN P.Nano capable of sub-micron tolerance. The diplexer is split into two halves with the E-plane cut and they are milled from brass. The milled blocks are coated with around 2 µm gold by electroplating. The diplexer is assembled with multiple screws as shown in Fig. 9(e). The weight of the CNC diplexer is 71.5 g (excluding the screws).

B. Surface treatment for the MLS printed diplexer

To improve the surface quality and performance of the diplexer, the MLS printed diplexer is plated with gold: Fig. 9(c) and Fig. 9(d) shows the assembly of the diplexer during the measurement. The stainless-steel base material and the fine iris structures of the diplexer makes the plating process difficult. The constituents of stainless-steel form an oxide layer on its surface preventing corrosion of the base metal, but also inhibiting good adhesion of a surface coating. The process utilizes an unconventional electroless plating method with gold plating over a nickel undercoat. To begin with, the diplexer surface undergoes electrolytic cleaning and Wood's nickel strike [42]. This is a conventional and proven method to remove the oxide layer and simultaneously apply a thin layer of nickel followed by electroless nickel plating and then the final gold plating. Time delay between these sequential processes is minimized. Otherwise, nickel may become passivated and further plating will be impossible, resulting in poor gold adhesion on the nickel strike. Moreover, both the cathodic cleaning and Wood's nickel strike works on the principle of electro-polishing/plating, which requires an anode, cathode, and direct current (DC). However, electro-plating would result in preferential plating on high current density areas (corners) and the surface will be uneven. In our work, the diplexer was plated using an electroless plating method which provides a uniform surface finish. The electroless plating also results in a better surface roughness which improves the effective conductivity of the inner surface. The workflow is illustrated in Fig. 10. The thickness of the nickel undercoat is about 3 µm and the gold layer is about 2 µm.

It should be noted that we have developed a plating process which can build up a thicker gold deposit than the conventional electroless nickel immersion gold (ENIG) process. In general,
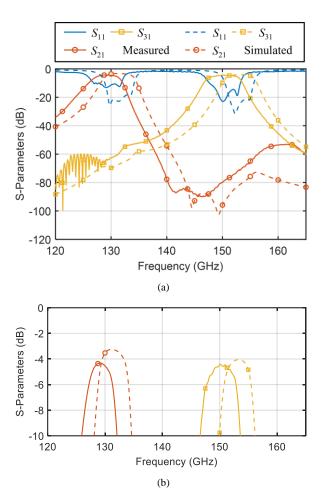
This article has been accepted for publication in IEEE Transactions on Components, Packaging and Manufacturing Technology. This is the author's version which has not been fully edited content may change prior to final publication. Citation information: DOI 10.1109/TCPMT.2022.3204887

6

(a)

(b)

Fig. 11. Measured and simulated S-parameter responses for the stainless-steel as-printed diplexer before gold coating.

Fig. 12. Surface roughness measurement on the bottom area of a selected waveguide cavity.

(a)   (b)

Fig. 13. Vertical dimension h measurement at locations 1, 2 and 3 (mm): 0.828, 0.834 and 0.837, respectively. Note the photograph is after gold coating. (a) A composite image formed by imaging on different levels. (b) The indication of h is a half of the cavity/waveguide height.

ENIG method is difficult to reach a thickness in excess of one micron. In this work, the final gold layer is plated from an autocatalytic chemistry, capable of plating a uniform and thick (2-3 µm) layer of gold with low surface roughness. There is very little literature on autocatalytic gold plating on stainless steel and rarely tested on 3D printed metal surfaces which have very different surface texture from the milled surfaces.

In addition, the iris structures in the diplexer aggravated the difficulty. Any bubbles formed during the plating process in the filter cavity will impede the plating process and therefore require careful agitation. A balance must be found between minimum flow required to replace depleted solution from the sample surface with fresh solution and turbulent flow that deprives the time for the gold to adhere to the surface. The plating rate used is approximately 2 hrs/µm and it is sensitive to bath parameters (such as agitation, pH, temperature, and impurities). Whilst these parameters can be frequently measured and adjusted as necessary, agitation, which is crucial for this plating chemistry, is set based on experience. We have not seen similar plating process used to treat the waveguide cavities before.
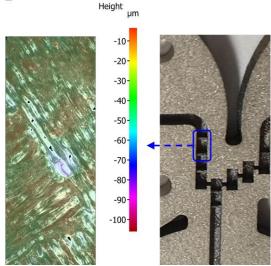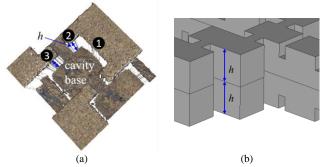
IV. MEASUREMENT AND DISCUSSION

A. Electrical performance of the stainless-steel MLS diplexer before gold coating

The S-parameter performance of the as-printed MLS diplexer was measured by using a Keysight network analyzer. Two ports of the diplexer connect with a pair of OML VNA extension modules, and the third port is terminated by a matched load. The measured S-parameter responses, compared with the simulation, are shown in Fig. 11. The simulation assumed the surface roughness of Sq = 2 µm (the surface characterization will be elaborated in Section IV(B)). With the nominal conductivity of the stainless steel, the effective conductivity will come down to 3.9×10^5 S/m due to the surface roughness [43]-[44]. Note that the effective conductivity is calculated by using Skin-Depth tool in CST Studio Suite with Rq. Since the Sq is an areal extrapolation of the equation of Ra, here the Sq value is direct applied. The simulated average insertion losses are 3.65 dB and 4.41 dB within the passbands for the Channel A and B, respectively. The simulated 3 dB bandwidths are 5.35 GHz and 5.23 GHz.

The measurement data shows the average insertion losses within the bandwidths for the two channels are 4.8 dB and 4.8

TABLE II.
MEASURED DIMENSIONS OF THE DIPLEXER IN COMPARISON WITH THEIR DESIGN VALUES

Dimension (µm)	Design values (µm)	Measured values (µm)	Deviations (µm)
W1	825.5	835	+9.5
W2	825.5	849	+23.5
W3	825.5	845	+19.5
W4	825.5	835	+9.5
W5	825.5	835	+9.5
W6	825.5	847	+21.5
W7	825.5	858	+32.5
W8	825.5	856	+30.5
WG1	825.5	831	+5.5
WG2	825.5	827	+1.5
L_1	958	N/A	N/A
L_2	1107	N/A	N/A
L_3	1654	1672	+18
L_4	1646	1658	+12
L_5	1355	N/A	N/A
L_6	1184	1204	+20
L_7	1096	1120	+24
L_8	969	984	+15

dB, broadly agreeing with the simulation. This is calculated from the S-parameter data over the range of 4 GHz around the measured center frequencies. The unloaded quality factor of the diplexer can be approximately extracted by using filter designer 3D in CST Studio Suite. Before gold plating, the estimated unloaded quality factors of the resonators in the two channels are 210 and 150, respectively. The downward center frequency shifts of the two channels are 2.8 GHz (2%) and 3.3GHz (2%). The measured 3 dB bandwidths are 5.0 GHz (−11%) and 6.0 GHz (+11%), respectively.

B. Surface characterization and dimensional measurement

To investigate the influence of the fabrication on the measurement results, the surface roughness and dimensions of the MLS diplexer have been measured using an Alicona optical system with a magnification of 50X [45]. The system has specified that the minimal measurable arithmetical mean height variation of the surface (Sa) is 0.06 µm and root-mean-square deviation of the surface (Sq) is 0.03 µm.

The surface roughness of the bottom surface of the waveguide cavity is measured as shown in Fig. 12. The measured Sa is 2.1 µm and Sq is 2.8 µm. A hatching pattern is discernible. It should be noted that no polishing was applied to the cavity for fear of damage to the fine iris structures. The surface roughness of 2 µm used in the simulation is an average from these measurements. The widths W and lengths L of the cavities, defined in Fig. 4(c), are also measured using Alicona optical system. The dimensions are given in Table II and compared to design values. It is noticed that the dimensions are generally 0.2 - 3.9% larger than the design which caused the downward frequency shift as shown in Fig. 11.

In addition to lateral dimensions, the depths of the cavities were also measured using the Alicona system. Fig. 13(a) shows a composite image formed by imaging on different levels. Here the measured quantity is h, half of the cavity/waveguide height as indicated in Fig. 13(b). The vertical dimension at the numbered locations is given in Fig. 13. They are slightly larger than the target values ($a/2 = 825.5$ µm) by less than 11 µm. This
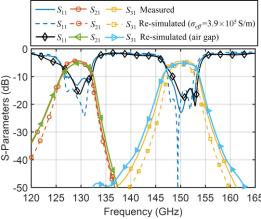

Fig. 14. Re-simulated S-parameter responses by considering the measured surface roughness, geometric dimensions and also the imperfect assembly contact, before gold coating.
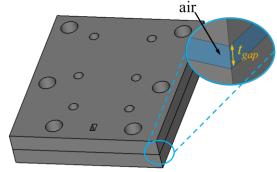

Fig. 15. The diplexer simulation model with an added air gap to investigate the effect of the assembly contact.

is only achievable due to the small layer thickness (7 µm) and powder particle size (5 µm) used in the printing process.

By considering the measured surface roughness and fabrication tolerances, we can refine and update the simulation model. All the design values are changed to the values shown in Table II. The unavailable values L_1, L_2 and L_5 are assumed to be 1.8% larger than the design values. The re-simulated response is shown in Fig. 14. Now that both the insertion loss level and frequency band match much better with the measurement, the discrepancy in return loss is still significant. Parameter study shows that this may be attributed to the imperfect contact between two half blocks of the diplexer. Using a model with a thin air gap between the two half blocks (Fig. 15), it has been found that the further re-simulated responses match the measured return loss much better, when this air gap is assumed to be $t_{gap} = 4$ µm, as shown in Fig. 14. It is not easy to measure the gap precisely, but such an air gap is plausible because no polishing has been applied to the contact surfaces.

C. Fabrication tolerance analysis

To investigate the influence of fabrication tolerance on the performance of the diplexer, an analysis has been performed based on simulation. The x and y directions of the diplexer shown in Fig. 7(a) are independently increased by 0 - 5%. Latin Hypercube sampling [46] with random distribution is utilized to collect 100 sets of design data for each direction. All the
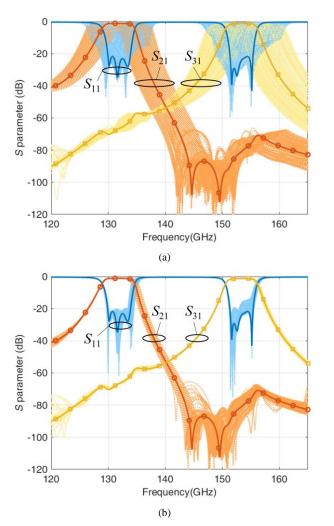
(a)

(b)

Fig. 16. The tolerance analysis of the diplexer with respect to the scaling in (a) *x*-direction and (b) *y*-direction.
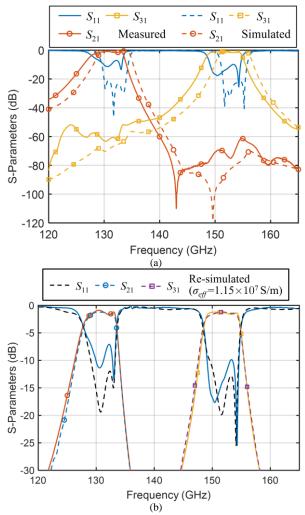

(a)

(b)

Fig. 17. (a) Measured and simulated S parameter responses for the MLS diplexer after gold plating. (b) Measured and re-simulated S-parameter responses considering the surface roughness after gold coating, measured geometric dimensions and imperfect assembly contact.

simulation results comparing with the initial responses are shown in Fig. 16.

It can be observed that the *x*-direction scaling affects more on the center frequency, bandwidth, and return loss. The bandwidth of channel A is more stable under *x*-direction scaling, while that of channel B is very sensitive. The *y*-direction scaling has less effect on the diplexer responses. As for the bandwidth variation under *y*-direction scaling, the channel B is more stable than channel A, because the scaling affects the inter-resonator couplings. Also, the *RL* of channel B is more sensitive to the *y*-direction scaling than that of channel A.

D. Measurement after gold coating

After gold plating, the diplexer was measured again using a pair of VDI frequency extension modules. The measured and simulated S-parameter responses are shown in Fig. 17(a). In the initial simulation, ideal conductivity of gold (4.6×10^7 S/m) is used. The simulated average insertion losses for the two channels are 0.49 dB and 0.57 dB, respectively. The measurement values are 1.31 dB and 1.37 dB. The extracted unloaded quality factor of the resonators in the two channels are 680 and 660, respectively. These are averaged over the range of

4 GHz around the measured center frequency. Note that gold coating has significantly reduced the insertion loss. It also reduces the frequency shift by a half to 1.22 GHz (0.9 %) and 1.69 GHz (1.1 %). The simulated 3 dB bandwidths are 5.66 GHz and 5.55 GHz while the measured 3dB bandwidths are 5.88 GHz (+3.9 %) and 6.39 GHz (+15.1%). Using the model in Fig. 14, simulation is repeated considering the measured surface roughness of 2 μm, measured geometric dimensions, and the imperfect assembly contact. It has been found again that the re-simulated S-parameter responses appear well-matched with the measured ones when the air gap is assumed to be $t_{gap} = 3.5$ μm, as shown in Fig. 17(b).

As a comparison, the measured S-parameter responses of the CNC machined diplexer are shown in Fig. 18. They agreed with the simulations extremely well without any tuning. The minimum insertion losses for the two channels are 0.60 dB and 0.49 dB. There is negligible frequency shifts while the bandwidths for the two channels are slightly widened by 0.51 GHz (+8.2%) and 0.63 GHz (10.1%). In Table III, the MLS diplexer and the CNC diplexer are compared with other reported sub-THz diplexers.
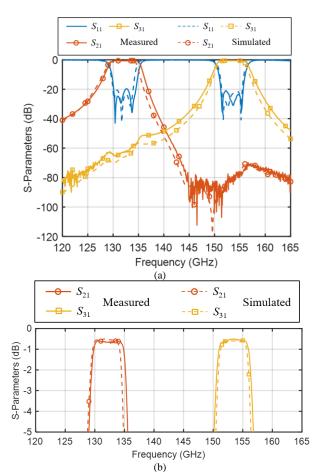
Fig. 18. Measured S parameter responses of the CNC milled diplexer comparing with the simulated responses.

TABLE III
COMPARISON OF DIPLEXER WITH PREVIOUSLY REPORTED NARROWBAND FILTERS AND DIPLEXERS

Ref.	f_0 (GHz)	Δf_0 (%)*	BW	ΔBW(%)*	IL(dB)*	Fabrication
[6]	132/145	0.7/1	3/5.1	7.5/8	1.2/0.8	DRIE
[7]	190/220	1.6/1.4	2.1/2.7	25/33	1.5/1.5	CNC
[9]	265/300	3/1.67	7.5/6.7	N/A	7.6/8	SU-8
T.W.*	132/153.5	0.92/1.1	4/4	3.9/15.1	1.31/1.37	MLS
T.W.*	132/153.5	0.2/0.17	4/4	8.2/10.1	0.60/0.49	CNC

* T.W. denotes this works.
* Δf_0 means center frequency shift, ΔBW is the bandwidth variation compared with the simulation results, IL denotes the measured average insertion loss within the specific bandwidths.

Weight: The parts fabricated by MLS can be much lighter than those by CNC. This is because 3D printing is more flexible. Topology optimization can be applied where no mechanical forces exist. Lighter parts should be cheaper to manufacture by MLS than by CNC milling. In this case, the printed diplexer is 18.2 g whereas the CNC diplexer is 71.5 g.

Fabrication tolerance: The tolerance of MLS is mainly determined by the printing resolution and layer thickness. This is still a challenge for 3D printing in general and can be refined to some extent in further iterations of the MLS. CNC has better stability in fabrication tolerance in general. In this case, the achieved dimensional deviation is about 30 μm for the printed diplexer. This is under 10 μm for the CNC diplexer.

Surface quality: The surface roughness from MLS (~ 2 μm for the diplexer) is much higher than that from CNC (typically 0.6 μm from the KERN P. Nano machine). This is one of the major disadvantages for 3D printing in general. Coating can mitigate this to some extent. New surface treatment methods are being developed to address this challenge. The adverse effect of surface quality could also be partially mitigated by design considerations.

Envelop size: For the MLS, the part size is still a limitation (60 mm × 60 mm × 30 mm for the printer used in this work). The printer is designed for small parts with fine structures. The CNC have a larger envelop size. However, in contrast to CNC micro milling, there is no need for specific fixture sets in MLS.

Scalability: In MLS, multiple parts can be manufactured simultaneously. In CNC machining, each part is usually manufactured separately, and operator actions are needed.

V. CONCLUSION

This paper presents a D-band diplexer fabricated by using a micro laser sintering (MLS) technique. The diplexer has an all-resonator structure, designed based on coupling matrix theory. The diplexer configuration and the dimensions have been tailored for fabrication constraints. A staircase coupling structure has been used to improve the isolation performance. This is the first time to use metal 3D printing technology for a multi-port filtering device at such a high frequency. The 3D printed diplexer has been compared with the same design implemented by high precision CNC milling. Comprehensive measurements have been carried out to characterize the diplexers. The reasons for the reduced performance of the MLS diplexer are attributed to surface roughness and fabrication

E. MLS versus high-precision CNC

At this stage, it is almost impossible to have enough reliable information to make a fair, general and quantified comparison between these two manufacture techniques because MLS printer is still very rare and under development.

Time-cost: The printing time is largely determined by the amount of material to be processed using MLS and the volume of the part. The '30 hr' in this case is not a typical time scale. This can be further optimized through topology optimization by removing unnecessary material as well as by applying device-specific process parameters such as layer thickness and laser power. Once the 3D printer is programmed, the fabrication can run until the end of manufacturing process. The high-precision CNC will not save much time considering the small radius of the cutting tool (~0.15 mm in this case) and the required human intervention especially for complex structures like the diplexer. For information, it took 11 hours programming, followed by 7 hours machining per complete block for this diplexer. Different cutting tools may be needed for different tolerance requirement in the waveguide part, e.g. the alignment pin/hole needing higher tolerance than the screw holes. One must also consider the tool wear and significant tooling cost for CNC. So, multiple complex factors should be considered for a fair comparison between the two technologies.

tolerance. An unconventional electroless gold plating method has been developed for the stainless-steel material and the challenging internal structures of the diplexer. Significant performance improvement is achieved after the gold coating. Compared with other reported sub-THz diplexers, comparable insertion loss has been achieved. The comparison in the frequency shift and bandwidth variation also indicates competitive fabrication tolerance of the MLS technique. The reference CNC milled diplexer demonstrated the best performance among all areas. The 3D-printed diplexer is a first iteration prototype. Its performance can be improved through further iterations (e.g., by enlarging/shrinking feature before printing to compensate for dimensional inaccuracies).

This investigation also revealed several limitations of the additive manufacturing technique in the context of sub-THz waveguide devices. The surface roughness is one intrinsic barrier for the AM technique. Better surface treatment technique is required to further enhance the functional performance of the printed parts. Dedicated plating process may be required to deal with unusual materials and challenging geometric structures. This work demonstrated an end-to-end process of the diplexer device. Although it still cannot compete with CNC machining in terms of achievable performance, the MLS process does offer a rapid prototyping capability, more possibilities and flexibilities in the design (such as integrated bend and irregular geometric structures) and potentially more integrated structures with reduced assembly need.

REFERENCES

[1] M. G. L. Frecassetti, A. Mazzanti, J. F. Sevillano, D. del Río and V. Ermolov, "D-Band Transport Solution to 5G and Beyond 5G Cellular Networks," 2019 European Conference on Networks and Communications (EuCNC), 2019, pp. 214-218.

[2] J. Doré et al., "Technology Roadmap for Beyond 5G Wireless Connectivity in D-band," 2020 2nd 6G Wireless Summit (6G SUMMIT), 2020, pp. 1-5.

[3] Electronic Communications Committee (ECC) within the European Conference of Postal and Telecommunications Administrations (CEPT), "The European table Of frequency allocations and applications in the frequency range 8.3 kHz to 3000 GHz (ECA TABLE)," Tech. Rep., October 2017.

[4] D. Gentina et al., "Millimetre Wave Transmission; Analysis of Spectrum, License Schemes and Network Scenarios in the D-band" ETSI GR mWT 008 V1.1.1, Aug. 2021. Available: http://www.etsi.org/standards-search.

[5] R. J. Cameron, C. M. Kudsia, and R. R. Mansour, "Multiplexer Theory and Design," *Microwave Filters for Communication Systems: Fundamentals, Design, and Applications*, Wiley, 2018, pp.569-608, ch18.

[6] X. Zhao, O. Glubokov, J. Campion, A. Gomez-Torrent, A. Krivovitca, U. Shah, and J. Oberhammer, "Silicon Micromachined D-Band Diplexer Using Releasable Filling Structure Technique," *IEEE Trans. Microw. Theory Techn.*, vol. 68, no. 8, pp. 3448-3460, Aug. 2020.

[7] X. Chen, J. Hu and X. Le, "G-Band Diplexer Based on E-Plane Waveguide Structures," *2018 Progress in Electromagnetics Research Symposium (PIERS-Toyama)*, 2018, pp. 1343-1346.

[8] W. Xia, X. Shang, and M. J. Lancaster, "All-resonator-based waveguide diplexer with cross-couplings," *Electronics Letters*, vol. 50, no. (25), pp: 1948-1950, 2014.

[9] T. Skaik, M. Lancaster, M. Ke, and Y. Wang, "A Micromachined WR-3 Band Waveguide Diplexer based on Coupled Resonator Structures," *Proc. 41st Eur. Microw. Conf.*, Oct. 2011, pp. 770–773.

[10] C. A. Leal-Sevillano, J. R. Montejo-Garai, J. A. Ruiz-Cruz, and J. M. Rebollar, "Low-loss Elliptical Response Filter at 100 GHz," *IEEE Microw. Wireless Compon. Lett.*, vol. 22, no. 9, pp. 459–461, Sep. 2012.

[11] X. Liao, L. Wan, Y. Yin, and Y. Zhang, "W-band Low-loss Bandpass Filter using Rectangular Resonant Cavities," *IET Microw., Antennas Propag.*, vol. 8, no. 15, pp. 1440–1444, Jul. 2014.

[12] C. A. Leal-Sevillano, T. J. Reck, G. Chattopadhyay, J. A. Ruiz-Cruz, J. R. Montejo-Garai, and J. M. Rebollar, "Development of a Wideband Compact Orthomode Transducer for the 180–270 GHz Band," *IEEE Trans. THz Sci. Technol.*, vol. 4, no. 5, pp. 634–636, Sep. 2014.

[13] J.-X. Zhuang, W. Hong, and Z. C. Hao, "Design and Analysis of A Terahertz Bandpass Filter," *Proc. IEEE Int. Wireless Symp. (IWS)*, Shenzhen, China, Mar./Apr. 2015, pp. 1–4.

[14] Y. Li, B. Pan, C. Lugo, M. Tentzeris, and J. Papapolymerou, "Design and Characterization of a W-band Micromachined Cavity Filter including a Novel Integrated Transition from CPW Feeding Lines," *IEEE Trans. Microw. Theory Techn.*, vol. 55, no. 12, pp. 2902–2910, Dec. 2007.

[15] D. Wang, M. J. Lancaster, Y. Wang, KM. Shum, and Q. Zhang, "WR-1.5 (500–750 GHz) waveguide bandpass filter fabricated using high precision computer numerically controlled machining." *Microw. Opt. Technol. Lett.*, vol. 63, pp: 1160– 1164, Dec. 2021.

[16] T. Kojima, A. Gonzalez, S. Asayama, and Y. Uzawa, "Design and Development of a Hybrid-Coupled Waveguide Multiplexer for a Multiband Receiver," *IEEE Trans. THz Sci. Technol.*, vol. 7, no. 1, pp. 10-19, Jan. 2017.

[17] Y. Li, B. Pan, C. Lugo, M. Tentzeris, and J. Papapolymerou, "Design and characterization of a W-band micromachined cavity filter including a novel integrated transition from CPW feeding lines," *IEEE Trans. Microw. Theory Techn.*, vol. 55, no. 12, pp. 2902–2910, Dec. 2007.

[18] X. H. Zhao, J. F. Bao, G. C. Shan, Y. J. Du, Y. B. Zhen, Y. Wen, and C. H. Shek, "D-band micromachined silicon rectangular waveguide filter," *IEEE Microw. Wireless Compon. Lett.*, vol. 22, no. 5, pp. 230–232, May 2012.

[19] C. A. Leal-Sevillano,T. J. Reck, C. Jung-Kubiak, G. Chattopadhyay, J. A. Ruiz-Cruz, J. R. Montejo-Garai, and J. M. Rebollar, "Silicon micromachined canonical E-plane and H-plane bandpass filters at the terahertz band," *IEEE Microw. Wireless Compon. Lett.*, vol. 23, no. 6, pp. 288–290, Jun. 2013.

[20] T. J. Reck, C. Jung-Kubiak, J. Gill, and G. Chattopadhyay, "Measurement of silicon micromachined waveguide components at 500–750 GHz," *IEEE Trans. Microw. Theory Techn.*, vol. 4, no. 1, pp. 33–38, Jan. 2014.

[21] J. R. Stanec and N. S. Barker, "Fabrication and integration of micromachined submillimeter-wave circuits," *IEEE Microw. Wireless Compon. Lett.*, vol. 21, no. 8, pp. 409–411, Aug. 2011.

[22] E. D. Cullens, L. Ranzani, K. J. Vanhille, E. N. Grossman, N. Ehsan, and Z. Popovic, "Micro-fabricated 130–180 GHz frequency scanning waveguide arrays," *IEEE Trans. Antennas Propag.*, vol. 60, no. 8, pp. 3647–3653, Aug. 2012.

[23] C. A. Leal-Sevillano, J. R. Montejo-Garai, M. Ke, M. J. Lancaster, J. A. Ruiz-Cruz, and J. M. Rebollar, "A pseudo-elliptical response filter at W-band fabricated with thick SU-8 photo-resist technology," IEEE Microwave Wireless Components Letters, vol. 22, no. 3, pp. 105–107, Mar. 2012.

[24] X. Shang, Y. Tian, M. J. Lancaster, and S. Singh, "A SU8 micromachined WR-1.5 band waveguide filter," *IEEE Microw. Wireless Compon. Lett.*, vol. 23, no. 6, pp. 300–302, Jun. 2013.

[25] X. Shang, M. Ke, Y. Wang, and M. J. Lancaster, "Micromachined W-band waveguide and filter with two embedded H-plane bends," *IET Microw., Antennas Propag.*, vol. 5, no. 3, pp. 334–339, Feb. 2011.

[26] M. Yata, M. Fujita, and T. Nagatsuma, "Diplexer for terahertz-wave integrated circuit using a photonic-crystal slab," *Proc. Microw. Photon. (MWP) 9th Asia–Pacific Microw. Photon. Conf. (APMP) Int. Topical Meeting*, Oct. 2014, pp. 40–43.

[27] J. Sun and F. Hu, "Three-dimensional printing technologies for terahertz applications: A review," *Int J RF Microw Comput Aided Eng*, vol. 30, no. 1, pp:e21983, 2020.

[28] X. Shang, P. Penchev, C. Guo, M. J. Lancaster, S. Dimov, Y. Dong, M. Favre, M. Billod, and E. de Rijk, "W-Band Waveguide Filters Fabricated by Laser Micromachining and 3-D Printing," *IEEE Trans. Microw. Theory Techn.*, vol. 64, no. 8, pp. 2572-2580, Aug. 2016.

[29] B. Zhang et al., "Metallic 3-D Printed Antennas for Millimeter- and Submillimeter Wave Applications," IEEE Transactions on Terahertz Science and Technology, vol. 6, no. 4, pp. 592-600, July 2016.

[30] M. Salek, X. Shang, R. C. Roberts, M. J. Lancaster, F. Boettcher, D. Weber, and T. Starke, "W-Band Waveguide Bandpass Filters Fabricated by Micro Laser Sintering," *IEEE Transactions on Circuits and Systems II: Express Briefs*, vol. 66, no. 1, pp. 61-65, Jan. 2019.

This article has been accepted for publication in IEEE Transactions on Components, Packaging and Manufacturing Technology. This is the author's version which has not been fully edited content may change prior to final publication. Citation information: DOI 10.1109/TCPMT.2022.3204887

11

[31] T. Skaik, M. Salek, Y. Wang, M. Lancaster, T. Starke and F. Boettcher, "180 GHz Waveguide Bandpass Filter Fabricated by 3D Printing Technology," 2020 13th UK-Europe-China Workshop on Millimetre-Waves and Terahertz Technologies (UCMMT), Tianjin, China, 2020, pp. 1-3.

[32] V. Fiorese, C. B. Gonçalves, C. del Rio Bocio, D. Titz, F. Gianesello, C. Luxey, G. Ducournau, E. Dubois, C. Gaquière, and D. Gloria, "Evaluation of Micro Laser Sintering Metal 3D-Printing Technology for the Development of Waveguide Passive Devices up to 325 GHz," 2020 IEEE/MTT-S International Microwave Symposium (IMS), Los Angeles, CA, USA, 2020, pp. 1168-1171.

[33] 3D Micro Print Gmbh. Accessed: Jul. 10, 2021. [Online]. Available: http://www.3dmicroprint.com/

[34] T. Skaik, M. Lancaster, and F. Huang, "Synthesis of Multiple Output Coupled Resonator Microwave Circuits using Coupling Matrix Optimization," *IET Microw., Antennas Propag.*, vol.5, no.9, pp. 1081-1088, Jun. 2011.

[35] X. Shang, Y. Wang, W. Xia, and M. J. Lancaster, "Novel Multiplexer Topologies Based on All-Resonator Structures," *IEEE Trans. Microw. Theory Techn.*, vol. 61, no. 11, pp. 3838-3845, 2013.

[36] Y. Yu, B. Liu, Y. Wang, M. J. Lancaster, and Q. S. Cheng, "A general coupling matrix synthesis method for all-Resonator diplexers and multiplexers," *IEEE Trans. Microw. Theory Techn.*, vol. 68, no. 3, pp. 987-999, March 2020.

[37] ITU-R Radio Regulation 2020. [Online]. Available: https://www.itu.int/en/myitu/Publications/2020/09/02/14/23/Radio-Regulations-2020

[38] D. Swanson and G. Macchiarella, "Microwave filter design by synthesis and optimization," in IEEE Microwave Magazine, vol. 8, no. 2, pp. 55-69, April 2007.

[39] J. -S. G. Hong and M. J. Lancaster, Microstrip Filters for RF/Microwave Application, vol. 167. Hoboken, NJ, USA: Wiley, 2004.

[40] R. J. Cameron, C. M. Kudsia, and R. R. Mansour, "Design and Physical Realization of Coupled Resonator Filters," Microwave Filters for Communication Systems: Fundamentals, Design, and Applications, Wiley, 2018, pp.457-484, ch14.

[41] J. F. Valencia Sullca, M. Guglielmi, S. Cogollos and V. E. Boria, "Hybrid wideband staircase filters in rectangular waveguide with enhanced out-of-band response," *IEEE Trans. Microw. Theory Techn.*, vol. 69, no. 8, pp. 3783-3796, Aug. 2021.

[42] H. Deng, and P. Moller, "Effects of pretreatment on the structure and properties of electroless nickel coatings." Plating and surface finishing, vol.81, no. 3, pp: 71-7, 1994.

[43] G. Gold and K. Helmreich, "A Physical Surface Roughness Model and Its Applications," *IEEE Trans. Microw. Theory Techn.*, vol. 65, no. 10, pp. 3720-3732, Oct. 2017.

[44] K. Lomakin, G. Gold, and K. Helmreich, "Analytical Waveguide Model Precisely Predicting Loss and Delay Including Surface Roughness," *IEEE Trans. Microw. Theory Techn.*, vol. 66, no. 6, pp. 2649-2662, June 2018.

[45] "Alicona optical system" [Online]. Available: https://www.alicona.com/our-technology/focus-variation/. [Accessed: 12-Aug-2021].

[46] J. F. Swidzinski and K. Chang, "Nonlinear statistical modeling and yield estimation technique for use in Monte Carlo simulations [microwave devices and ICs]," *IEEE Trans. Microw. Theory Techn.*, vol. 48, no. 12, pp. 2316-2324, Dec. 2000.

Yang Yu (Member, IEEE) was born in Tianjin, P.R. China, in 1991. He received the B.Eng. degree in communication engineering and the M.Eng. degree in information and communication engineering at Tianjin Polytechnic University, Tianjin, P.R.China, in 2013 and 2016, respectively, and Ph.D. degree in electronic and electrical engineering from University of Birmingham, Birmingham, Edgbaston, U.K., in 2022. He was also a joint Ph.D. student with Southern University of Science and Technology (SUSTech), Shenzhen, P.R.China.

He is current a Special Research Assistant with Key Laboratory of Microwave Remote Sensing, National Space Science Center, Chinese Academy of Sciences, Beijing. He is also an Honorary Research Fellow with the Emerging Device Technology Group, University of Birmingham. His current research interests include synthesis and design of RF/microwave components, 3D printed and micromachined MMW/THz devices and computational intelligence techniques for engineering.

Yi Wang (M'09–SM'12) was born in Shandong, China. He received the B.Sc. degree in applied physics and M.Sc. degree in condensed matter physics from the University of Science and Technology, Beijing, China, in 1998 and 2001, respectively, and the Ph.D. degree in electronic and electrical engineering from the University of Birmingham, Edgbaston, Birmingham, U.K., in 2005. From 2004 to 2011, he was a Research Fellow at the University of Birmingham. In 2011, he became a Senior Lecturer and then Reader at the University of Greenwich, U.K.. He is currently an Associate Professor with the University of Birmingham. He is the author of over 170 research papers. He has been the reviewer of several major microwave, antenna and sensor journals and an Associate Editor of IET MAP. He serves the TPC Chair of 2021 European Microwave Conference. His current research interests include multiport filtering networks, filter-antenna integration, millimeter-wave and terahertz antennas and devices for metrology, communication, and sensing. He is particularly interested in working with new materials and various novel manufacturing techniques, such as micromachining and 3D printing, for RF/microwave applications.

Talal Skaik received M.Sc. degree in communications engineering and Ph.D. degree in microwave engineering from the University of Birmingham, Birmingham, U.K., in 2007 and 2011, respectively.

After PhD, he worked in lecturing in electrical engineering until 2019. He is currently working as a research fellow in the Electronic, Electrical and Systems Engineering Department at the University of Birmingham. His research interests include microwave filters and antennas, 3D-printed microwave devices, temperature compensated filters for satellite payloads, multi-port coupled resonator structures and energy harvesting circuits.

Thomas Starke was born in Mittweida, Germany in 1978. He received Diploma in Mechanical Engineering from Chemnitz University of Technology in 2002. After working as project manager in automotive industry and hardware developer at 3D-Micromac AG, in 2013 he took over the position as Head of Development at 3D MicroPrint GmbH in Chemnitz, Germany.

Xiaobang Shang (Senior Member, IEEE) received the B.Eng. degree (Hons.) in electronics and communication engineering from the University of Birmingham, Birmingham, U.K., in 2008, the B.Eng. degree in electronics and information engineering from the Huazhong University of Science and Technology (HUST), Wuhan, China, in 2008, and the Ph.D. degree in microwave engineering from the University of Birmingham, in 2011. He is currently a Senior Research Scientist with the National Physical Laboratory, Teddington, U.K.

He has authored or coauthored more than 90 scientific articles on microwave measurements and microwave circuits. Dr. Shang was a recipient of the ARFTG Microwave Measurement Student Fellowship Award in 2009 and the IEEE Tatsuo Itoh Award in 2017. He is a member of IEEE MTT-3 and MTT-21 Technical Committees and an Associate Editor for the IEEE Microwave and Wireless Components Letters. Dr. Shang is the Representative of Group 4 countries (UK, Ireland, Gibraltar, Malta) on the European Microwave Association (EuMA) General Assembly, for a three-year term (2022-2024).

Michael J. Lancaster (SM'2004) was born in England in 1958. He was educated at Bath University, UK, where he graduated with a degree in Physics in 1980. His career continued at Bath, where he was awarded a PhD in 1984 for research into non-linear underwater acoustics.

After leaving Bath University he joined the surface acoustic wave (SAW) group at the Department of Engineering Science at Oxford University as a Research Fellow. The research was in the design of new, novel SAW devices, including RF filters and filter banks. In 1987 he became a Lecturer at The University of Birmingham in the Department of Electronic and Electrical Engineering, lecturing in electromagnetic theory and microwave engineering. Shortly after he joined the department he began the study of the science and applications of high temperature superconductors, working mainly at microwave frequencies. He was promoted to head of the Department of Electronic, Electrical and Systems Engineering in 2003. His present personal research interests include microwave filters and antennas, as well as the high frequency properties and applications of a number of novel and diverse materials. This includes micromachining as applied to terahertz communications devices and systems.

Professor Lancaster is Fellow of the IET and UK Institute of Physics. He is a Chartered Engineer and Chartered Physicist. He has served on MTT IMS technical committees. Professor Lancaster has published two books and over 200 papers in refereed journals.
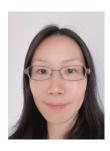
Peter Hunyor holds a BEng (Hons) and a diploma in natural sciences. Certified Airline and Aerospace surface finisher by NASF (National Association for Surface Finishing, USA). Joined the Science and Technology Facilities Council (STFC) as a process engineer in 2015 and has been working on various surface finishing and inspection techniques ever since. He is managing the gold-plating & electro-forming laboratory and the materials analysis laboratory within the MMT Group. Currently working on the European Space Agency (ESA's) MetOp project where he successfully validated multiple surface finishing processes for flight. His current research interest include additive manufacturing and high precision electroforming to develop corrugated feedhorns.

Peter G. Huggard received the BA(Mod) honours graduate degree in experimental physics from Trinity College Dublin, Ireland in 1987. This was followed by a PhD degree on the generation and detection of short pulsed terahertz radiation. After postdoctoral research at the Universities of Regensburg, Germany, and Bath, U.K., and two years lecturing in physics at the University of Bath, he joined the CCLRC Rutherford Appleton Laboratory in 2000. Dr Huggard is currently a UK Research Councils' Individual Merit Fellow, and Leader of the Millimetre Wave Technology Group at the STFC Rutherford Appleton Laboratory. His research interests cover technology for active and passive remote sensing of the earth's atmosphere and radio astronomy. He works on new terahertz technology development within the Group, working on detectors, sources, filters, instruments, and instrument calibration technology. He has authored more than 60 refereed publications and acts as a referee for several international physics and engineering journals. Dr. Huggard is a Chartered Physicist and also a Senior Member of the OSA. He also holds a visiting professorship at the Department of Electrical and Electronic Engineering, University College London, UK.

Hui Wang received her MSc and PhD degree in astrophysics and space instrumentation from University Pierre and Marie Curie, Paris, France in 2005 and 2009 respectively. She joined RAL Space in 2009 as a Millimetre Wave Design Scientist/Engineer and works as a key member of the Millimetre Wave Technology Group. She is currently leading Schottky diode device development within the Group. Her general interests include millimetre wave and THz devices, primarily heterodyne frequency mixers and harmonic up-conversion multipliers, in support of Earth observation and astronomy remote sounding experiments.

Michael Harris, photograph and biography not available at the time of publication.

Mat Beardsley, photograph and biography not available at the time of publication.

Qingsha S. Cheng (S'00–M'05–SM'09) is currently an associate professor with the Department of Electrical and Electronic Engineering, Southern University of Science and Technology (SUSTech), Shenzhen, China. He is also with Shenzhen Key Laboratory of EM Information. He received the B.Eng. and M. Eng. from Chongqing University, China, in 1995 and 1998, respectively. He received his Ph.D. at McMaster University, Canada, in 2004. In 1998, he was with the Department of Computer Science and Technology, Peking University, China. In 2004, he joined the Department of Electrical and Computer Engineering, McMaster University as a post-doctoral fellow, and then research associate and lecturer. In 2014, he joined SUSTech as an assistant professor. His research interests include smart modelling and optimization of microwave components and antennas, surrogate modelling and optimization, multi-objective optimization, and neural networks. He has authored or co-authored more than 200 publications in book chapters, international technical journals, and refereed conference proceedings. His research is funded by the National Natural Science Foundation of China (NSFC) and the Ministry of Science and Technology (MOST) of China.